Published in final edited form as:
J Mol Cell Cardiol. 2013 July ; 60: 151–160. doi:10.1016/j.yjmcc.2013.04.021.

Altered regional cardiac wall mechanics are associated with differential cardiomyocyte calcium handling due to nebulette mutations in preclinical inherited dilated cardiomyopathy

K Maiellaro-Rafferty[1], **JP Wansapura**[2], **U Mendsaikhan**[1], **H Osinska**[1], **J James**[1], **MD Taylor**[1], **J Robbins**[1], **EG Kranias**[3], **JA Towbin**[1], and **E Purevjav**[1]

[1]The Heart Institute, Department of Pediatrics, Cincinnati Children's Hospital Medical Center, Cincinnati, OH

[2]Department of Radiology, Imaging Research Center, Cincinnati Children's Hospital Medical Center, Cincinnati, OH

[3]Department of Pharmacology and Cell Biophysics, University of Cincinnati, College of Medicine, Cincinnati, OH

Abstract

Background—Nebulette (NEBL) is a sarcomeric Z-disc protein involved in mechanosensing and force generation via its interaction with actin and tropomyosin-troponin complex. Genetic abnormalities in *NEBL* lead to dilated cardiomyopathy (DCM) in humans and animal models.

Objectives—To determine the earliest preclinical mechanical changes in the myocardium and define underlying molecular mechanisms by which *NEBL* mutations lead to cardiac dysfunction.

Methods and Results—We examined cardiac function in 3-month-old non-transgenic (non-Tg) and transgenic (Tg) mice (WT-Tg, G202R-Tg, A592E-Tg) by cardiac magnetic resonance (CMR) imaging. Contractility and calcium transients were measured in isolated cardiomyocytes. A592E-Tg mice exhibited enhanced *in viv*o twist and untwisting rate compared to control groups. *Ex vivo* analysis of A592E-Tg cardiomyocytes showed blunted calcium decay response to isoproterenol. CMR imaging of G202R-Tg mice demonstrated reduced torsion compared to non-Tg and WT-Tg, but conserved twist and untwisting rate after correcting for geometric changes. *Ex vivo* analysis of G202R-Tg cardiomyocytes showed elevated calcium decay at baseline and a conserved contractile response to isoproterenol stress. Protein analysis showed decreased α-actinin and connexin43, increased cardiac troponin I phosphorylation at baseline in G202R-Tg, providing a molecular mechanism for enhanced *ex vivo* calcium decay. Ultrastructurally, G202R-

Corresponding Author: Enkhsaikhan Purevjav, MD, PhD. Enkhsaikhan.Purevjav@cchmc.org Mailing address: MLC 7020, 3333 Burnet Avenue, Cincinnati, OH 45229.

Author Contributions: K.M-R maintained all animals, acquired the *ex vivo* and protein expression data, analyzed CMR images, and prepared all figures and text for this manuscript. JW acquired and analyzed CMR images. UM analyzed electron microscopy images, performed immunohistochemical and protein analyses. HO acquired and analyzed the electron microscopy images. JJ performed echocardiography. MDT and JR edited this manuscript. EGK provided equipment and input on the cardiomyocyte contractile mechanics and calcium transient data and edited the manuscript. JAT and EP supervised all experimentation and edited this manuscript.

Disclosures: none declared

Tg cardiomyocytes exhibited increased I-band and sarcomere length, desmosomal separation, and enlarged t-tubules. A592E-Tg cardiomyocytes also showed abnormal ultrastructural changes and desmin downregulation.

Conclusion—This study showed distinct effects of *NEBL* mutations on sarcomere ultrastructure, cellular contractile function, and calcium homeostasis in preclinical DCM *in vivo*. We suggest that these abnormalities correlate with detectable myocardial wall motion patterns.

Keywords

nebulette; dilated cardiomyopathy; sarcomere; cardiac magnetic resonance imaging; troponin; connexin43; desmin

1. Introduction

Approximately 30–50% of patients with various forms of cardiomyopathy and a large “at risk” population consisting of healthy relatives of patients with cardiomyopathy exhibit inherited mutations in genes encoding cardiomyocyte sarcomeric, Z-disc, desmosomal, and cytoskeletal proteins. Most pediatric (66%) dilated cardiomyopathy (DCM) cases are idiopathic [1] and individuals carrying sarcomeric gene mutations may not present clinical signs of cardiomyopathy until adulthood, supporting a temporal mechanism by which chronically altered mechanosensing and mechanotransduction lead to cardiomyopathy. Currently, mutation identification via genetic screening is not a reliable predictor of the cardiomyopathy phenotype or severity. Different cardiomyopathy clinical phenotypes can be observed in individuals or family members carrying the same gene mutations, particularly when the genetic abnormality is in a gene encoding a multifunctional protein. Moreover, cardiac function and symptoms of congestive heart failure (CHF) at the time of DCM diagnosis can be prognostic for death and cardiac transplantation rates in children. An increase in the risk of death and cardiac transplantation by 2.2-fold was evident in DCM cases with moderate left ventricular (LV) systolic dysfunction as compared to patients with normal LV systolic function, suggesting that recognition and diagnosis of DCM at the preclinical or subclinical stages is important in terms of potentially impacting outcome [1]. In addition, approximately one third of the asymptomatic “at risk” population have serum anti-heart autoantibodies at baseline, one third has echocardiographic abnormalities, such as LV enlargement and depressed fractional shortening (FS), and the remainder of such relatives develop DCM [2]. This suggests that apparently healthy relatives may have latent, early, or undiagnosed disease. Delineation of “preclinical” alterations in cardiac function or defining useful biomarkers would be extremely useful in correlating early effects of genetic abnormalities to development of a cardiomyopathy phenotype.

We and others have used cardiovascular magnetic resonance (CMR) imaging to detect occult alterations in regional myocardial wall motion in early manifestations of DCM and CHF [3]. Recent clinical echocardiography data show that early diastolic dysfunction, despite normal LV size and ejection fraction (EF), can be captured during the preclinical stage of DCM [4]. Thus, advanced cardiac imaging and computation of regional wall mechanics may open a window into our understanding of subclinical cardiomyopathic events, prediction of disease development and outcome.

Alterations in cardiomyocyte calcium regulation and morphology are linked to cardiac mechanical behavior and, upon detection, may expose preclinical events associated with DCM. Failing human myocardium expresses decreased calcium handling proteins and the proportion of calcium flux through intracellular and extracellular calcium stores is modified [5]. Mechanical stretch increases intracellular calcium in cardiomyocytes [6] and cardiac overload-induced hypertrophy is attenuated by calcium-dependent proteins, such as

calcineurin and CaMKII [7]. Furthermore, thin filament calcium sensitivity is directly coupled to cardiomyocyte physiologic contractility [8]. Genetic variations in sarcomeric proteins may thus reveal themselves as changes in calcium signaling prior to presenting a detectable cardiomyopathy phenotype.

Nebulette (*NEBL*), which encodes a sarcomeric Z-disc protein, contributes to muscle force generation via its interaction with actin and cardiac tropomyosin/troponin (cTm/cTn) complex, as well as participating in force transmission of the cardiac myofibril via the Z-disc assembly [9]. Humans carrying either A592E-NEBL or G202R-NEBL mutation manifest DCM. Transgenic mice with cardiomyocyte-restricted expression of either human mutant (A592E-Tg and G202R-Tg, respectively) develop DCM at 6 months of age [10]. The G202R-NEBL mutation is localized in the nebulin-repeat region that extends into the I-band, while the A592E-NEBL mutation resides nearest the sarcomeric Z-disc (Figure 1). In part due to their distinct locations, these two NEBL mutations are thought to lead to DCM by different mechanisms *via* mutation-induced alterations in protein-protein interactions.

In this study, we hypothesized that G202R mutation affects the interaction of the NEBL protein with the cTm/cTn complex, and may lead to early mechanical dysfunction by destabilizing the calcium-cTn interaction, while the A592E mutation may alter Z-disc mechanosensing. To differentiate the earliest mutation-specific mechanistic basis of DCM, our objective was to correlate these molecular and cellular changes with occult subclinical alterations in cardiac function that could serve as diagnostic predictors for the DCM phenotype onset. The ultimate significance of this study is to advance development of tools for improved prevention and clinical management of cardiac disease, particularly by identifying and treating the disease at its earliest stages. Our data show differential calcium-mediated mechanisms of cardiac function in A592E-Tg and G202R-Tg NEBL mutant hearts. Furthermore, our data suggest that CMR strain analysis of myocardial untwisting rate may serve as a sensitive functional indicator of cardiac dysfunction in the preclinical stage of murine DCM.

2. Methods

2.1 Animals

The transgenic mice with specific cardiomyocyte expression of mutant human, G202R-Tg and A592E-Tg, NEBL develop DCM at 6 months after birth [10]. In this study, 3-month-old G202R-Tg and A592E-Tg mice and non-transgenic (non-Tg) littermates were investigated. To confirm expression of NEBL transgene at 3-month-old hearts as well as to exclude possible “unstable” cardiac transgene expression, Western blot analysis was performed prior to planned studies. As a control for transgene expression, age-matched mice with specific cardiomyocyte expression of wild-type human NEBL (WT-Tg) were used. All procedures were approved by the Cincinnati Children’s Hospital Medical Center Institutional Animal Care and Use Committee and were in compliance with the standards for the *Care and Use of Laboratory Animals*, Institute of Laboratory Animal Resources, National Academy of Sciences, Bethesda, MD.

2.2 Functional assessment with echocardiography and CMR imaging

Cardiac function was assessed by echocardiography and CMR imaging. Mice were anesthetized with 1.5–2.5% isofluorane. Echocardiograms were obtained with a Vevo 770 High-Resolution In Vivo Micro-Imaging System and RMV 707B Scanhead (VisualSonics Inc). Left ventricle (LV) dimensions, including end-diastolic and end-systolic dimensions (LVED and LVES, respectively), interventricular septal thickness in diastole and systole (IVSd and IVSs, respectively) and LV posterior wall thickness in diastole and systole

(LVPWd and LVPWs, respectively) were measured directly. Fractional shortening (FS), EF and the LVPW to wall thickness ratios in systole and diastole were then calculated.

CMR was performed as previously described [11]. Tagged images were acquired in the basal and apical levels in the short axis plane. Tagged images were analyzed using HARP (Diagnosoft Plus, Diagnosoft Inc., CA, USA) to assess the ventricular rotation. Ventricular dimensions were calculated using Segment v1.x (http://segment.heiberg.se, E. Heiberg, In Proceedings of IEEE Computers in Cardiology 2005). LV torsion, ρ, was calculated as rotation in degrees (°) of the heart apex relative to the base and LV twist was calculated as torsion normalized by a geometric constant, as described previously [12]. Ventricular dimensions were calculated using Segment v1.x (http://segment.heiberg.se, E. Heiberg, In Proceedings of IEEE Computers in Cardiology 2005). LV twist was calculated as

$$Geometric\ constant=(r_{apex}+r_{base})/2l \quad \text{Equation (1)}$$

$$Twist=\rho \times Geometric\ constant \quad \text{Equation (2)}$$

where r is the radius of base and apex, l is the length between apical and base CMR images, and ρ is torsion. As recoil of torsion, or LV untwisting, is independent of left atrial pressure, it is considered a sensitive measure of LV diastolic function [12, 13]. Therefore, untwisting rate was calculated as the maximum of the derivative of ρ with respect to time and normalized for geometric changes by the geometric constant.

2.3 Transmission Electron Microscopy

Ultrastructural analysis was performed as previously described [14]. Briefly, hearts were fixed by perfusion with 3.5% glutaraldehyde in cardioplegic buffer for 2 minutes, followed by 3.5% glutaraldehyde in 100 mM cacodylate buffer (pH 7.3) for 2 minutes. The fixatives were introduced into the heart through the apex and next through the right ventricle. To prevent pressure build up in the LV, the aorta, vena cava, and pulmonary veins were cut immediately after the heart started to inflate with fixative. Hearts were dissected into fragments and fixed in 1% glutaraldehyde/2% paraformaldehyde overnight at 4°C. Tissue fragments were post-fixed on ice in 1% O_sO_4 in cacodylate buffer, dehydrated in acetone, and embedded in a Poly/Bed 812 resin mixture. Sections were counterstained with uranyl acetate and lead citrate and examined on a Zeiss 912 transmission electron microscope at an accelerating voltage of 100 kV.

2.4 Isolation of cardiomyocytes from adult mice

Adult male mice (12–14 weeks) were anesthetized by pentobarbital (100 mg/kg) and heparinized (5,000 U/kg). Hearts were quickly removed, cannulated at the aorta by Langendorff mode, and perfused with Tyrode perfusion buffer (120.4 mM NaCl, 14.7 mM KCl, 10 mM Na-HEPES, 0.6 mM K_2HPO_4, 0.6 mM Na_2HPO_4, 1.2 mM $MgSO_4$, 4.6mM $NaHCO_3$, 5.5 mM Glucose, 30 mM taurine, and 10 mM butane-dione bonoxime; pH 7.4) for 10 min. Subsequently, hearts were perfused with an enzyme solution (Tyrode containing 0.35 mg/ml Liberase TH (Roche- 05401151001) and 12.5 μM Ca) for 15 min or until heart became flaccid. Left ventricular tissue was excised, minced, pipette dissociated and filtered through a 200 μm 200um nylon mesh (Spectrum Labs, 146487). Digestion was stopped with Tyrode wash solution (plus 12.5 uM Ca, 10% bovine calf serum). Myocytes settled by gravity and were sequentially washed in 25 uM, 100uM, 200 uM, and 1mM Ca^{2+}-Tyrode wash solution, and resuspended in 1.8mM Ca^{2+}-Tyrode for further analysis.

2.5 Measurement of contractility and intracellular calcium transients in adult cardiomyocytes

To measure contractility, cardiomyocyte in 1.8mM Ca^{2+}-Tyrode were placed on a chamber positioned on the stage of an inverted microscope (Nikon Diaphot 200). The experiments were performed at room temperature. Contraction was field-stimulated by a Grass S5 stimulator (0.5 Hz, square waves). Peak rates of contraction and relaxation were measured by edge detection. For calcium signal measurement, cardiomyocytes were incubated with the acetoxymethyl ester form of fura-2 (Fura-2/AM; 2 μM (2.5ng/ml)) for 30 min at room temperature, in the dark, with gentle shaking. Myocytes were then resuspended in 1.8 mM Ca^{2+}-Tyrode solution. In the chamber positioned on the inverted microscope stage, the cells were alternately excited at 340 and 380 nm by a Delta Scan dual-beam spectrophotofluorometer (Photon Technology) and Ca^{2+} transient was recorded as the 340/380 nm ratio of the resulting 510-nm emissions. Contractility and calcium transients were also collected in the presence of isoproterenol (Iso, 50nM). All data were analyzed using software from FeliX and Ionwizard. Ten to fifteen cells from each heart (n= 4–13 hearts) were measured for contractility and another ten were measured for calcium transients.

2.6 Protein expression and localization analysis

Protein expression in the heart was quantified by Western Blotting. Ventricular tissues were homogenized with beads (Precellys 24, Bertin technologies) in RIPA buffer (50mM Tris-cl pH 7.4, 150mM NaCl, 1% NP40, 1mM PMSF, and protease and phosphatase inhibitor cocktails (Roche)). Protein concentration was determined by Bradford Assay (BioRad) and equal amounts (7–30 μg) of protein were separated on 13% SDS-polyacrylamide gels. Proteins were transferred to nitrocellulose membranes and blocked with either 5% milk or BSA. Membranes were incubated overnight at 4°C in 1% milk in TBS-T with antibodies for GAPDH (Santa Cruz), NEBL (provided by Dr. Labiet), calsequestrin (CSQ), cTnI, phosphorylated cTnI at Ser23/24 (pTnI), protein kinase A (PKA, Cell Signaling), SERCA (polyclonal rabbit anti-SERCA provided by Dr. Kranias), phospholamban (PLN, Affinity Bioreagents, Inc.), phosphorylated PLN at Ser16 and Thr17 (pPLN, Badrilla), sodium-calcium exchanger (NCX, Thermo), connexin43 (Cx43, Sigma), N-cadherin, desmin, and α-actinin (Abcam). Membranes were then incubated for 1 hour with horseradish peroxidase (HRP)-conjugated secondary antibody (1:5000). Secondary antibodies were activated with ECL Plus solution (GE Healthcare), immunoblots were imaged using a Typhoon Scanner and band intensity was analyzed with image J software.

Immunohistochemical analysis was performed to study localization of proteins using antibodies described above. Cardiac muscle sections (5μm) were obtained from frozen whole hearts, blocked for 30 min using Cas-Block (Zymed), then, incubated with primary antibodies (30 min) followed by incubation with secondary antibodies for 1hour at room temperature. Immunoreactivity was visualized by confocal microscopy (Nikon).

2.7 *In vitro* kinase assay

Kinase activity in heart lysates was analyzed using the Kinase-Glo Plus luminescent kinase assay (Promega, Madison, WI). Human cTnI substrate (20ng) was used as the phosphorylation substrate in the presence of 5 ug total heart lysate and 10uM ATP in kinase reaction buffer (40mM Tris, pH 7.5, 20mM MgCl2, and 0.1mg/ml BSA). Activity was measured by quantifying the amount of ATP remaining in solution following the kinase reaction. The reaction was performed on a 96-well plate in parallel with standard control reactions of 0–10 units of cAMP-dependent protein kinase, catalytic subunit (Promega).

2.8 Statistical Analysis

Data are presented as mean ± SE. Statistical analyses were performed using GraphPad5 Prism software. Data were analyzed by ANOVA or Mann-Whitney test and Bonferonni post tests were used for post hoc analyses. $P < 0.05$ was considered significant. Analyses details are provided in each figure legend.

3. Results

3.1 Mutation-specific differences in myocardial twist are detected in the preclinical stage using CMR strain analysis

We performed echocardiography and CMR to assess cardiac function and remodeling in 3-months-old non-Tg and Tg mice. Echocardiography did not reveal differences in cardiac function, chamber dimensions, or myocardial thickness among groups (Supplemental Table 1). Given that overt changes in FS and EF were not detected by echocardiography, these data support the definition of 3 months after birth as a “preclinical” stage prior to clinical DCM phenotype, which occurs at 6 months in this model [10]. To detect occult subclinical functional abnormalities, tagged CMR was performed. Heart rates (Figure 2A) were similar across groups. Indicative of DCM [15], torsion, ρ, the rotation of the apex with respect to the base, was significantly lower ($p<0.05$) in G202R-Tg mice compared to both non-Tg and WT-Tg mice (Figure 2B). To determine if geometric changes in heart structure underlined this difference in torsion, the geometric constant was calculated (Equation 1). Hearts from both mutant groups were more spherical than non-Tg hearts (Figure 2C). To correct for these geometric changes, apical twist was calculated according to Equation 2. Peak systolic apical twist in non-Tg, WT-Tg, and G202R-Tg mice was approximately 5° (Figure 2D), which is a higher twist value than reported by Henson *et al* [16], but lower than that reported by Zhou *et al* [17]. A592E-Tg twist was significantly elevated compared to both non-Tg and WT-Tg (Figure 2D), indicating transiently accentuated systolic function in this model. This finding is corroborated by other murine models with sarcomeric gene mutations that show transiently increased systolic function before development of DCM [18]. Untwisting rate was higher in the A592E-Tg mutant compared to WT-Tg (Figure 2E). Taken together, these baseline CMR data suggest that A592E-Tg and G202R-Tg models exhibit different *in vivo* mechanical function in the preclinical stage of DCM.

3.2 Isolated cardiomyocyte contractility and intracellular calcium transients expose distinct underlying functional behavior in NEBL mutants

To determine whether differences in CMR parameters correlate with mechanical events at the cellular level and serve as sensitive preclinical indicators of cardiac dysfunction, contractility and intracellular calcium transients in isolated, live cardiomyocytes were examined. At baseline (Figure 3A and C and E, left columns), the cardiomyocyte contractile mechanics such as %FS and rate of contraction were the same in all groups. Rate of relaxation (Figure 3D) is significantly different in the two mutants.

To clarify mechanisms of these differences, the amplitude of intracellular calcium release and the calcium decay rate were also examined in isolated cardiomyocytes. At baseline (Figure 3B and F and H, left columns), the calcium amplitude was the same in all groups. Baseline calcium decay rate (Figure 3G) was increased in G202R-Tg cardiomyocytes compared to WT-Tg. This increase was not coupled to increased baseline G202R-Tg cardiomyocyte relaxation rate (Figure 3D), as typically expected.

Isoproterenol (Iso) treatment was used to determine whether alteration in relaxation rate correlated to decreased myofilament cTnI sensitivity (Figure 3A and C–D, right columns). Significantly increased fractional shortening and rates of contraction and relaxation were

seen in all groups except A592E-Tg (Figure 3D–E). The Iso-induced calcium decay rate also increased to a lesser extent in the A592E-Tg group compared to other groups (Figure 3G). Isolated cardiomyocyte studies also indicated that A592E-Tg cardiomyocytes are shorter than G202R-Tg cardiomyocytes (Figure 3H). These data suggest that A592E-Tg mutants have normal calcium handling at baseline, but incomplete calcium cycling during Iso-mediated stress. In contrast, the G202R-Tg mutant may have reduced myofilament calcium sensitivity at baseline, as suggested by increased calcium decay rate, while the isotropic response to Iso stimulation is preserved.

3.3 Alterations in cTnI phosphorylation proteins are detected in G202-Tg mutants

To further determine whether the faster baseline calcium decay in the G202R-Tg mutants was the result of decreased myofilament sensitivity to calcium at baseline, expression of Ser^{23}/Ser^{24} phosphorylated cTnI to total cTnI protein was examined in heart lysates from 3-months old mice. The ratio of Ser^{23}/Ser^{24} phosphorylated cTnI (pTnI) to total cTnI was significantly increased in G202R-Tg hearts compared to WT-Tg and A592E-Tg (Figure 4A–B). This data provided a possible molecular mechanism for both the increased calcium decay rate and preserved response to Iso-induced stress observed in this mutant *ex vivo*, and for the preserved *in vivo* twist detected by CMR.

To investigate whether altered calcium sequestration into the SR underscored the differences in calcium decay in the mutant groups, expression of the calcium handling proteins SERCA2a, NCX and PLN was examined (Figure 4A). SERCA2a and NCX steady state levels, as well as the ratio of Ser^{16}-PLN to total PLN pentamer, were unchanged across all groups, suggesting normal SR reuptake in NEBL mutants. Together, these protein data demonstrate that altered cTnI phosphorylation is detectable in the G202R-Tg mutant only during preclinical DCM.

3.4 Protein kinase activity is elevated in NEBL G202R-Tg mutant hearts

Abnormal high levels of protein kinases activities may partially increase phosphorylation of cTnI in cardiomyocytes [19]. To investigate whether increased phosphorylation of cTnI in hearts from G202R-Tg mice is conferred by increased PKA activity, heart lysates were analyzed for PKA expression and total kinase activity. Protein expression of the active monomeric subunit of PKA C-alpha was not changed among groups (Figure 4A). However, total kinase activity on a cTnI substrate, measured by the production of ADP in the presence of 10μM ATP, was enhanced in G202R-Tg heart lysates (5μg) (Figure 4C). These data indicate that increased cardiac kinase activity may underlie the increase in Ser^{23}/Ser^{24} phosphorylated cTnI detected in the G202R-Tg mutant.

3.5 Sarcomeric, cell-cell contact, and t-tubule ultrastructure is altered in mutant hearts

Previous ultrastructural investigation of clinical DCM in NEBL models found focal intercalated disc separation in hearts from 6 months old G202R-Tg mice [10]. To determine whether cardiomyocyte and sarcomere morphology is altered at the ultrastructural level in preclinical DCM, TEM analysis of LV myocardial sections was performed in 3-month-old mice. Sarcomeric Z-disc morphology appeared normal in all groups (Figure 5A–H). Focal loss of desmosome integrity and cell-membrane dissociation was observed in myocardium from G202R-Tg (Figure 5F, arrows), and to a lesser extent, in A592E-Tg mice (Figure 5H). Both mutants showed degenerated vesicular structures (asterisks) at the intercalated discs. G202R-Tg myocardium showed lateralized and enlarged t-tubules (Figure 5E, arrowheads), further suggestive of interrupted calcium handling [20]. Dimensional analysis revealed increased sarcomere length in G202R-Tg cardiomyocytes compared to all other groups (Figure 5I) and increased I-band in the G202R and A592E-Tg groups compared to non-Tg (Figure 5J). A592E-Tg sarcomeres were shorter than G202R-Tg (Figure 5I), which supports

shorter A592E-Tg cardiomyocytes detected in *ex vivo* isolated myocyte preparation (Figure 3H). Altered cardiomyocyte and sarcomere dimensions have been shown in skeletal muscle from a nebulin knock-out mouse [21].

To examine alterations in structural, t-tubule and cell-cell contact proteins, we further quantified Cx43, Cav3, N-cadherin, desmin, and a-actinin expression and studied their localization in the heart using Western blotting and immunohistochemistry, respectively. Expression of Cx43 and α-actinin was decreased in G202R-Tg heart lysates, while desmin was decreased in lysates from A592E-Tg hearts (Figure 4A–B). Desmin (Figure 6, left columns, red) and α-actinin (data not shown) localization was not affected in all groups, while Cx43 mislocated in the lateral border in both G202R-Tg and A592E-Tg cardiomyocytes as indicated in green (Figure 6E and G, arrows). N-cadherin, a cell-cell adhesion marker, and Cav3, a t-tubule marker, were examined to detect occult reinforcement of the intercalated disc and t-tubules, respectively, but were not found upregulated. Interestingly, mislocated Cx43 was co-localized with Cav3 in both mutants (Figure 6F and H) suggesting possible underlying causes of t-tubule and gap junction disorganization.

Taken together, these data suggest that cardiomyocyte ultrastructure alterations are mutation-specific and distinctive at preclinical stage of the disease. The G202R mutation, located in the I-band nebulin-repeat modules, led to sarcomere lengthening, enlarged t-tubules and cell-cell contact disorganization. The A592E-Tg mutation, located near the Z-disc, caused structural abnormalities in the intercalated disc, although not to the extent of the G202R-Tg mutation.

4. Discussion

The objective of this study was to determine whether molecular and mechanical alterations correlate with early signs of cardiac mechanical behavior in murine models of DCM due to inherited *NEBL* mutations. NEBL is thought to be a mechano-receptive protein in the Z-disc [9] and our previous studies dissected the mechanosensing and mechanotransducing functions of the protein using *NEBL* transgenic murine models, G202R-Tg and A592E-Tg, which develop DCM at 6 months [10]. The hypothesis of current study was that distinct *NEBL* mutations induce DCM via different domain specific mechanisms and that insight into the preclinical mechanisms leading to DCM may be obtained by investigation of the mutant mice at an earlier time point. Our data showed that, in preclinical murine DCM, both *NEBL* mutations alter sarcomeric protein expression and localization, which differentially effect calcium handling or mechanical response to stress. In addition, we show that occult diastolic dysfunction due to these molecular changes can be detected by noninvasive CMR imaging.

The major phenotypic differences found in *NEBL* transgenic mutant mice compared to non-Tg and WT-Tg controls at 3 months of age are summarized in Table 1. Hearts from 3-month-old G202R-Tg mice show structural alterations in geometry, increased t-tubule area, lateralization of Cx43, downregulation of α-actinin and Cx43, sarcomere & I-band lengthening, and desmosomal separation at the intercalated disc. Evaluation of calcium transients in isolated G202R-Tg cardiomyocytes showed an increase in baseline calcium decay rate, which is supported at the molecular level by increased cTnI phosphorylation and protein kinase activity. These molecular mechanisms likely underlie the conservation of systolic twist and untwisting rate detected *in vivo* by CMR. On the other hand, the major preclinical changes discovered in A592E-Tg mice were downregulation of desmin, lateralization of Cx43, blunted *ex vivo* Iso-induced calcium decay rate in isolated cardiomyocytes, and increased *in vivo* cardiac twist and untwisting rate, Our data support the developing paradigm that genetic mutations have distinct effects on protein function

depending on the location of the mutation within the gene. This study provides evidence that noninvasive CMR imaging is a powerful clinical resource to associate alterations in cardiac torsion and twist to genotype-phenotype correlation. It also provides novel association pathways between NEBL, its binding partners, and cardiomyocyte cell-cell coupling.

Our noninvasive CMR results show that alterations in cardiac torsion and twist can be detected in preclinical DCM in *NEBL* mutant mice. These data are, to our knowledge, the first to differentiate genotype and cardiac phenotype using CMR imaging as a noninvasive clinical tool to detect occult cardiac mechanical changes. Individuals carrying sarcomeric gene mutations may express clinical signs of DCM and heart failure many years after birth. Enhanced detection of preclinical disease is, therefore, critical for prevention and clinical management of DCM. Echocardiography and CMR imaging both provide cardiac dimensions and global function, but current opinion is that wall motion and untwisting rate may be more prognostically useful parameters [3, 22]. Tissue Doppler echo provides myocardial strain rate, whereas CMR provides total wall strain, which is debatably a more relevant metric to link cardiac function to genotype [23]. Twist is a parameter of wall motion that may directly correlate with myocardial potential energy available for systolic contraction. Arising from the oblique myofiber orientation within the myocardium [24], the LV twists in systole, storing potential energy that is released during diastolic untwisting. This untwisting reflects both the passive mechanics of the myocardium and ATP hydrolysis at the myosin head. Our data show that G202R-Tg mutants maintain twist and untwisting rate near non-Tg and WT-Tg levels via increased cTnI phosphorylation and geometric remodeling. A592E-Tg mutants, however, do not share these preclinical alterations, but demonstrated elevated *in vivo* cardiac twist and untwisting rate. In addition, isolated A592E-Tg cardiomyocytes did not increase contractility or calcium cycling in response to Iso treatment. These data suggest that A592E-Tg hearts function at maximum isotropic mechanical ability in preclinical DCM. Although increased cardiac function is typically representative of hypertrophic CM (HCM), 5–10% of patients with HCM ultimately exhibit progression into a dilated phase [25]. In addition, other murine models with mutations in sarcomeric genes such as desmin, *MyH7, MyBPC, and cTNT* also exhibit transiently increased systolic function before developing DCM [26, 27]

Analysis of *ex vivo* isolated cardiomyocytes and myocardial protein expression in the *NEBL* Tg mice allowed dissection of the effect of distinct genetic mutations on NEBL protein function in the cardiomyocyte. The G202R mutation is located in the thin filament-binding nebulin-repeat modules [22] at the N-terminal (Figure 1). The N-terminal repeats are responsible for the maintaining the interactions of NEBL with F-actin and cTm/cTn complex within the I-band, suggesting that N-terminal *NEBL* mutations promote cardiac dysfunction by destabilizing the interaction of calcium with the thin filament-cTm/cTn complex. Our data support NEBL mutation-associated alteration of the cTm/cTn complex, as shown by enhanced cTnI phosphorylation and increased calcium decay rate in the G202R-Tg mutant. Failing human hearts typically show increased calcium handling protein levels [5], possibly to compensate for dysfunctional stretch-sensing at the sarcomeric Z-disc. The G202R-Tg mutant showed more rapid decay of calcium after systole in isolated cardiomyocytes, but did not show the expected corresponding increase in diastolic relaxation rate. Uncoupling between troponin calcium sensitivity and cell relaxation, however, has been reported in human carriers of DCM mutations [4] and in the murine cTnC-G159D mutation model of DCM [28]. In this model, the cTnC-G159D mutation altered Ca(2+)-binding to cTnC modulating myofilament mechanics in the presence of phosphorylated cTnI. Indeed, increased cTnI phosphorylation was detected in G202R-Tg heart lysates. We consider that future studies on the cross-bridge cycling rate in isolated cardiomyocyte studies at physiologic temperature may unmask increased cardiomyocyte relaxation rate. Overall, our data suggest that increased cTnI phosphorylation underlies

enhanced calcium decay rate and preservation of homeostatic heart function in the presence of mutated G202R-NEBL. Increased phosphorylation of cTnI may be caused by altered interaction of the mutant G202R-NEBL protein with the cTm/cTn complex and increased total kinase activity on cTnI.

Analysis of the G202R *NEBL* mutation also reveals a potential association between sarcomeric NEBL and cell-cell integrity. The data show that NEBL mutated at G202R results in downregulation of α-actinin, the Z-disc cross-linking protein, and Cx43, the predominant connexins in gap junction of ventricular myocardium (Figure 4B). Regulation of Cx43 is dependent on numerous factors such as mechanical and biochemical stress, hypertrophic remodeling, and heart failure, involving activation of different signaling pathways [29]. Decrease in expression and translocation of Cx43 are reported to have profound effects on cardiac function and is linked to sudden death due to DCM and conduction abnormalities [30]. Thus, Cx43 downregulation and lateralization may serve as marker for diagnosis of early signs of cardiomyopathic remodeling that progress to clinical DCM seen at 6 months of age in this model. It also provides mechanisms for increase of cTnI phosphorylation and total kinase activity on cTnI in preclinical stage.

The pathogenesis pathway to DCM in A592E-Tg mice is distinct from G202R mutants. The A592E *NEBL* mutation is located in the C-terminal nebulin-repeat modules closest to the mechanosensing Z-disc (Figure 1). C-terminal NEBL mutations are thought to alter Z-disc mechanosensing and anchoring to the cell membrane. Mutated NEBL at A592E induced downregulation of desmin protein and associated loss of cardiomyocyte architecture. Interestingly, desmin-null mice develop early cardiomyocyte hypertrophy followed later by ventricular dilation [27], which supports the enhanced systolic function detected by CMR in the preclinical stage of DCM in this mutant. In addition, loss of desmin staining in patients with idiopathic DCM is typically predictive of unfavorable prognosis [31]. Previous work in our lab showed loss of desmin in a DCM patient carrying the Q128R-*NEBL* mutation [10]. Indeed, diminished desmin expression in the A592E-Tg mutant supports our previous postulation that interactions at the SH3 domain of NEBL anchoring α-actinin, vinculin, and myopalladin with desmin [32], transmit information from the Z-disks to the intermediate filaments maintaining the structural and functional integrity of myocytes. SH3 is a C-terminal domain in the modular structure of nebulin family members, and it is closer in proximity to NEBL A592E than to NEBL G202R (Figure 1). Thus, we propose that the A592-NEBL mutation alters the interaction with desmin and loss of cohesion between the Z-disc and the sarcolemma through intermediate filaments, promoting DCM *via* desminopathy mechanisms.

Lastly, our overexpression murine models may not clearly represent the physiological human DCM phenotype compared to knock-in models that are ideal for recapitulating human genetic mutations. However, the robust comparative study of two *NEBL* mutants with WT-Tg and non-Tg littermates exposed mechanistic and functional data to delineate the mutation-specific contributions to cardiac pathophysiology that ultimately lead to common clinical DCM phenotype.

5. Conclusion

In summary, we provide novel functional and molecular mechanisms in preclinical inherited DCM that arise due to distinct sarcomeric Z-disc mutations. We suggest that distinct mutations in the *NEBL* gene lead to dysfunctional mechanosensing at the Z-disc and differential regulation of calcium-signaling. In addition, we provide novel data that molecular changes are correlated with occult changes in ultrastructural EM and myocardial

wall motion and demonstrate these changes can be detected by advanced imaging prior to overt changes in cardiac output or fractional shortening.

Supplementary Material

Refer to Web version on PubMed Central for supplementary material.

Glossary

NEBL	nebulette
DCM	dilated cardiomyopathy
CMR imaging	cardiac magnetic resonance imaging

References

1. Towbin JA, Lowe AM, Colan SD, Sleeper LA, Orav EJ, Clunie S, et al. Incidence, causes, and outcomes of dilated cardiomyopathy in children. Jama. 2006 Oct 18; 296(15):1867–76. [PubMed: 17047217]
2. Caforio AL, Mahon NG, Baig MK, Tona F, Murphy RT, Elliott PM, et al. Prospective familial assessment in dilated cardiomyopathy: cardiac autoantibodies predict disease development in asymptomatic relatives. Circulation. 2007 Jan 2; 115(1):76–83. [PubMed: 17179019]
3. Hagenbuch SC, Gottliebson WM, Wansapura J, Mazur W, Fleck R, Benson DW, et al. Detection of Progressive Cardiac Dysfunction by Serial Evaluation of Circumferential Strain in Patients With Duchenne Muscular Dystrophy. The American Journal of Cardiology. 2010; 105(10):1451–5. [PubMed: 20451693]
4. Lakdawala NK, Thune JJ, Colan SD, Cirino AL, Farrohi F, Rivero J, et al. Subtle Abnormalities in Contractile Function Are an Early Manifestation of Sarcomere Mutations in Dilated Cardiomyopathy/Clinical Perspective. Circulation: Cardiovascular Genetics. Oct 1; 2012 5(5):503–10. [PubMed: 22949430]
5. Bers DM. Calcium Fluxes Involved in Control of Cardiac Myocyte Contraction. Circulation Research. 2000 Aug 18; 87(4):275–81. [PubMed: 10948060]
6. Kudoh S, Akazawa H, Takano H, Zou Y, Toko H, Nagai T, et al. Stretch-modulation of second messengers: effects on cardiomyocyte ion transport. Progress in Biophysics and Molecular Biology. 82(1–3):57–66. [PubMed: 12732268]
7. Lim HW, De Windt LJ, Steinberg L, Taigen T, Witt SA, Kimball TR, et al. Calcineurin Expression, Activation, and Function in Cardiac Pressure-Overload Hypertrophy. Circulation. 2000 May 23; 101(20):2431–7. [PubMed: 10821822]
8. Solaro RJ, Kobayashi T. Protein phosphorylation and signal transduction in cardiac thin filaments. J Biol Chem. 2011 Mar 25; 286(12):9935–40. [PubMed: 21257760]
9. Moncman CL, Wang K. Targeted disruption of nebulette protein expression alters cardiac myofibril assembly and function. Experimental cell research. 2002 Feb 15; 273(2):204–18. [PubMed: 11822876]
10. Purevjav E, Varela J, Morgado M, Kearney DL, Li H, Taylor MD, et al. Nebulette Mutations Are Associated With Dilated Cardiomyopathy and Endocardial Fibroelastosis. Journal of the American College of Cardiology. 2010; 56(18):1493–502. [PubMed: 20951326]
11. Wansapura JP, Millay DP, Dunn RS, Molkentin JD, Benson DW. Magnetic resonance imaging assessment of cardiac dysfunction in δ-sarcoglycan null mice. Neuromuscular Disorders. 2011; 21(1):68–73. [PubMed: 20934875]
12. Seldrum S, Pierard S, Moniotte S, Vermeylen C, Vancraeynest D, Pasquet A, et al. Iron overload in polytransfused patients without heart failure is associated with subclinical alterations of systolic left ventricular function using cardiovascular magnetic resonance tagging. J Card Mag Res. 2011; 13:23.

13. Dong S-J, Hees PS, Siu CO, Weiss JL, Shapiro EP. MRI assessment of LV relaxation by untwisting rate: a new isovolumic phase measure of τ. American Journal of Physiology - Heart and Circulatory Physiology. 2001 Nov 1; 281(5):H2002–H9. [PubMed: 11668061]
14. Sadayappan S, Gulick J, Osinska H, Martin LA, Hahn HS, Dorn GW, et al. Cardiac Myosin-Binding Protein-C Phosphorylation and Cardiac Function. Circulation Research. 2005 Nov 25; 97(11):1156–63. [PubMed: 16224063]
15. Rüssel I, Götte M. New insights in LV torsion for the selection of cardiac resynchronisation therapy candidates. Netherlands Heart Journal. 19(9):386–91. [PubMed: 21562790]
16. Henson RE, Song SK, Pastorek JS, Ackerman JJH, Lorenz CH. Left ventricular torsion is equal in mice and humans. American Journal of Physiology - Heart and Circulatory Physiology. 2000 Apr 1; 278(4):H1117–H23. [PubMed: 10749705]
17. Zhou R, Pickup S, Glickson JD, Scott CH, Ferrari VA. Assessment of global and regional myocardial function in the mouse using cine and tagged MRI. Magnetic Resonance in Medicine. 2003; 49(4):760–4. [PubMed: 12652548]
18. Nanni L, Pieroni M, Chimenti C, Simionati B, Zimbello R, Maseri A, et al. Hypertrophic cardiomyopathy: two homozygous cases with atypical hypertrophic cardiomyopathy and three new mutations in cases with progression to dilated cardiomyopathy. Biochemical and Biophysical Research Communications. 2003; 309(2):391–8. [PubMed: 12951062]
19. Endoh M. Cardiac Ca2+ signaling and Ca2+ sensitizers. Circ J. 2008 Dec; 72(12):1915–25. [PubMed: 18981594]
20. Orchard CH, Pásek M, Brette F. The role of mammalian cardiac t-tubules in excitation-contraction coupling: experimental and computational approaches. Exp Phys. 2009 May 1; 94(5):509–19.
21. Witt CC, Burkart C, Labeit D, McNabb M, Wu Y, Granzier H, et al. Nebulin regulates thin filament length, contractility, and Z-disk structure in vivo. EMBO J. 2006; 25(16):3843–55. [PubMed: 16902413]
22. Sherazi S, Zaręba W. Diastolic heart failure: predictors of mortality. Cardiol J. 2011; 18(3):222–32. [PubMed: 21660911]
23. To ACY, Dhillon A, Desai MY. Cardiac Magnetic Resonance in Hypertrophic Cardiomyopathy. JACC: Cardiovascular Imaging. 2011; 4(10):1123–37. [PubMed: 21999873]
24. Lorenz, Ch; Fau-Pastorek, JS.; Pastorek, Js; Fau-Bundy, JM.; Bundy, JM. Delineation of normal human left ventricular twist throughout systole by tagged cine magnetic resonance imaging. J Cardiovasc Magn Reson. 2000; 2(2):97–108. [PubMed: 11545133]
25. Biagini E, Coccolo F, Ferlito M, Perugini E, Rocchi G, Bacchi-Reggiani L, et al. Dilated-hypokinetic evolution of hypertrophic cardiomyopathy: prevalence, incidence, risk factors, and prognostic implications in pediatric and adult patients. Journal of the American College of Cardiology. 2005 Oct 18; 46(8):1543–50. [PubMed: 16226182]
26. Nanni L, Pieroni M, Chimenti C, Simionati B, Zimbello R, Maseri A, et al. Hypertrophic cardiomyopathy: two homozygous cases with “typical” hypertrophic cardiomyopathy and three new mutations in cases with progression to dilated cardiomyopathy. Biochem Biophys Res Commun. 2003 Sep 19; 309(2):391–8. [PubMed: 12951062]
27. Milner DJ, Taffet GE, Wang X, Pham T, Tamura T, Hartley C, et al. The Absence of Desmin Leads to Cardiomyocyte Hypertrophy and Cardiac Dilation with Compromised Systolic Function. Journal of Molecular and Cellular Cardiology. 1999; 31(11):2063–76. [PubMed: 10591032]
28. Biesiadecki BJ, Kobayashi T, Walker JS, John Solaro R, de Tombe PP. The Troponin C G159D Mutation Blunts Myofilament Desensitization Induced by Troponin I Ser23/24 Phosphorylation. Circulation Research. 2007 May 25; 100(10):1486–93. [PubMed: 17446435]
29. Teunissen BE, Jongsma HJ, Bierhuizen MF. Regulation of myocardial connexins during hypertrophic remodelling. Eur Heart J. 2004 Nov; 25(22):1979–89. [PubMed: 15541833]
30. Chen X, Zhang Y. Myocardial Cx43 expression in the cases of sudden death due to dilated cardiomyopathy. Forensic science international. 2006 Oct 16; 162(1–3):170–3. [PubMed: 16887310]
31. Pawlak A, Gil RJ, Grajkowska Wa, Nasierowska-Guttmejer AM, Rzezak Ja, Kulawik T. Significance of Low Desmin Expression in Cardiomyocytes in Patients With Idiopathic Dilated Cardiomyopathy. The American journal of cardiology. 111(3):393–9. [PubMed: 23178054]

32. Purevjav E, Arimura T, Augustin S, Huby AC, Takagi K, Nunoda S, et al. Molecular basis for clinical heterogeneity in inherited cardiomyopathies due to myopalladin mutations. Hum Mol Genet. 2012 May 1; 21(9):2039–53. [PubMed: 22286171]

Highlights

1. Mutations in the same gene lead to cardiomyopathy via different mechanisms.
2. Changes to compensate cardiacfunction are detectable in preclinical DCM.
3. CMRstrain analysis can detect early indicators of cardiac dysfunction.

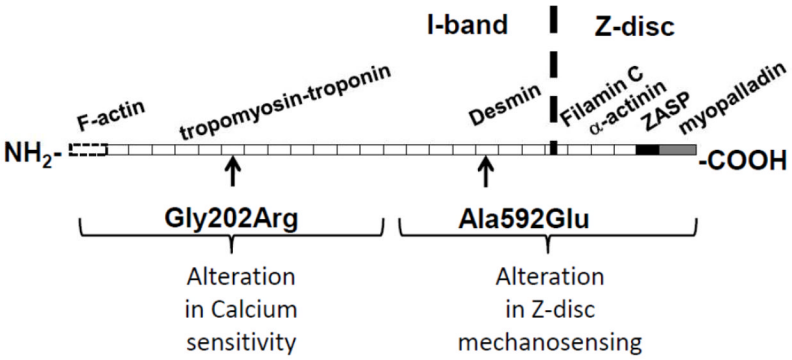

Figure 1. Structure of NEBL protein and its interacting partners

The G202R mutation is located in the force-transducing nebulin-repeat modules at the N-terminal, while the A592E mutation is located in the C-terminal nebulin-repeat modules closest to the Z-disc. The functional domains are indicated as follows: dotted rectangle - F-actin binding domain; white rectangles - nebulin repeats; black - linker domain; grey - SH3 domain. Interacting proteins are shown to the corresponding binding nebulin repeats and domains.

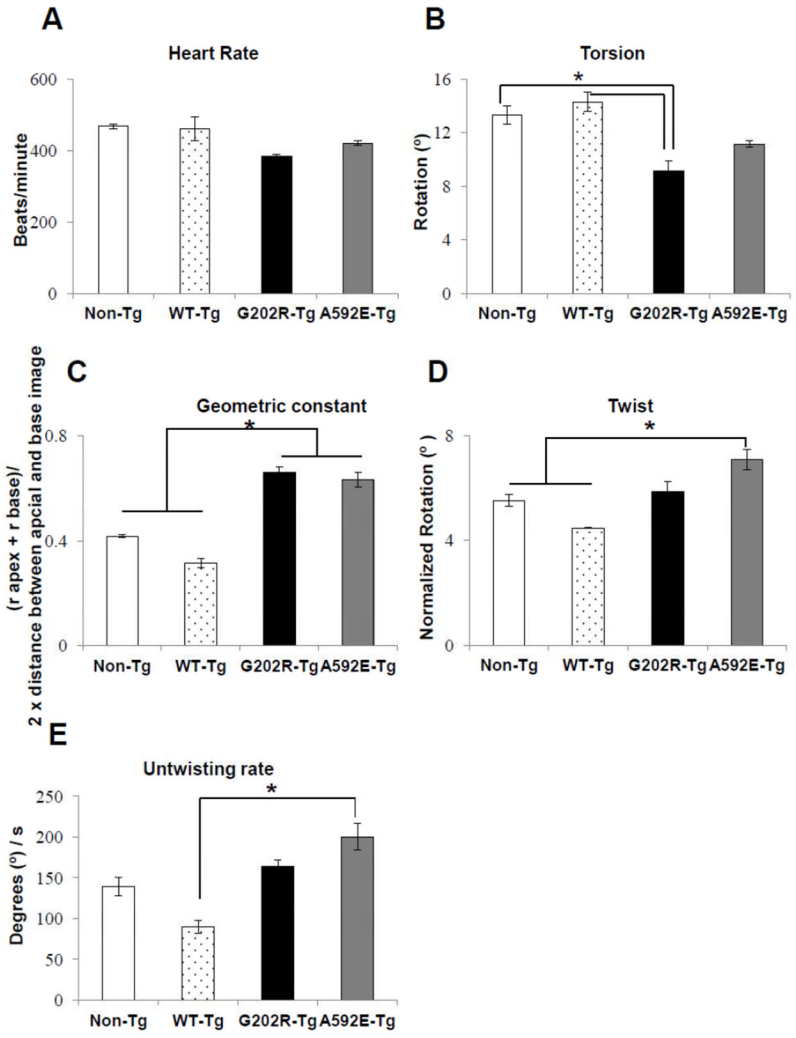

Figure 2. Assessment of cardiac function by CMR imaging

A) Heart rate in anesthetized mice was similar among the 4 groups during CMR imaging. B) Torsion, the rotation of the heart apex with respect to the base, was reduced in the G202R-Tg group compared to controls. C) The geometric constant, ratio of LV length to the LV inner radius during diastole, indicated a rounded phenotype in the mutants compared to controls. D) Twist, torsion corrected for LV geometric remodeling, was elevated in the A592E-Tg mutant compared to non-Tg and WT-Tg. E) Untwisting rate, a diastolic function indicator, remained elevated in the A592E-Tg group compared to WT-Tg. N= 4 animals in non-Tg, G202R-Tg, and A592E-Tg. N=2 in WT-Tg. Data analyzed by Mann-Whitney t-test. *=$P<0.05$.

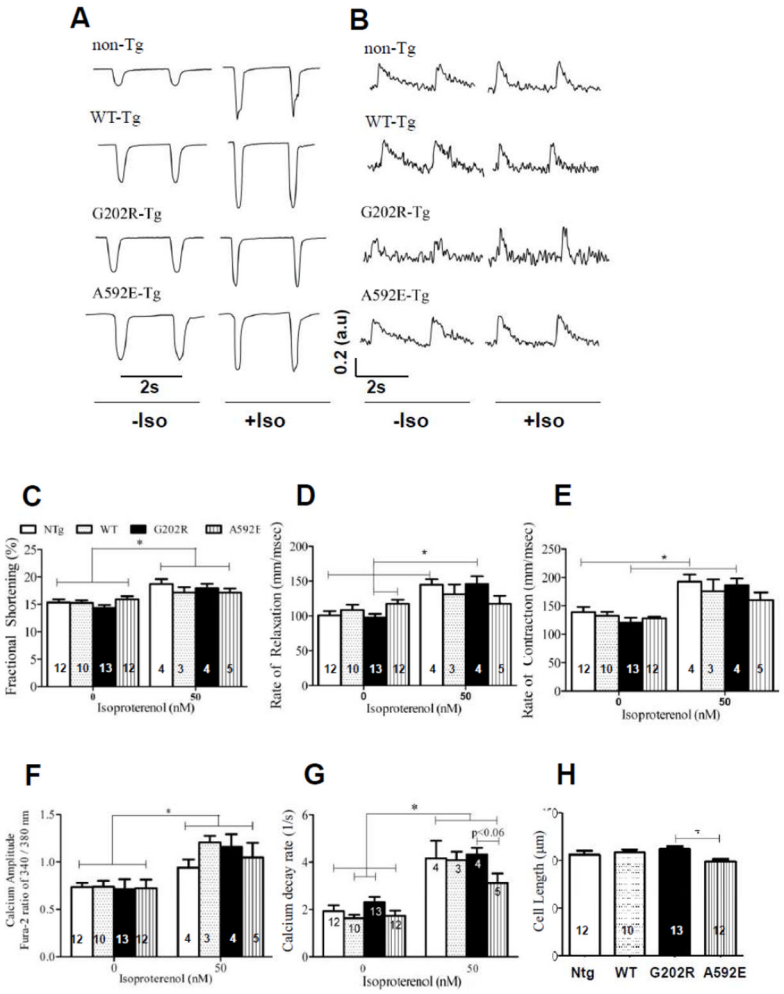

Figure 3. *Ex vivo* contractility and calcium transients of isolated cardiomyocytes from adult mice

A) Representative traces illustrating myocyte contractions at 0.5 Hz stimulation in non-Tg, WT-Tg, G202R-Tg, and A592E-Tg cardiomyocytes with and without Iso (50nM) stimulation. B) Representative traces illustrating $Ca2^{+}$ transients measured with fura-2AM in all groups, while stimulated with 0.5 Hz, with and without Iso treatment. C) Cardiomyocyte fractional shortening presented in fractional shortening percentage (FS%) in non-Tg (white bar), WT-Tg (dotted bar), G202R-Tg (black bar) and A592E-Tg (vertical striped bar) mice. Left set of bars represents FS% at baseline, right set of bars indicate a significant increase in the cardiomyocyte FS% after Iso treatment in all groups. D) Rate of relaxation represented in mm/msec indicates significant disparity in two mutants at baseline (left bars). Iso-mediated mechanical stress (right set of bars) increased rate of relaxation in non-Tg and G202R-Tg cells, but not in A592E-Tg cells. E) Increase of rate of contraction to isoproterenol represented in mm/msec was diminished in A592E-Tg cells compared to other groups, which showed significant increase in rate of contraction to Iso stress. F) Calcium amplitude was the same in all groups at baseline (left bars) and increased to similar levels after Iso treatment (right bars). G) Increased baseline calcium decay (l/s) was observed in G202R-Tg cells compared to other groups, particularly, the difference was statistically significant from the WT-Tg. Iso treatment enhanced calcium decay in all groups, but to a lesser degree in the A592E-Tg cells (right bars). H) Length of isolated cardiomyocytes indicated in μm. Cardiomyocytes from A592E-Tg mice are shorter than G202R-Tg.

Numbers in bars indicate the N number of animals per group. 10–15 cells per heart were examined. Data analyzed by ANOVA with Bonferroni post-test and pair wise t-test. *=$P<0.05$.

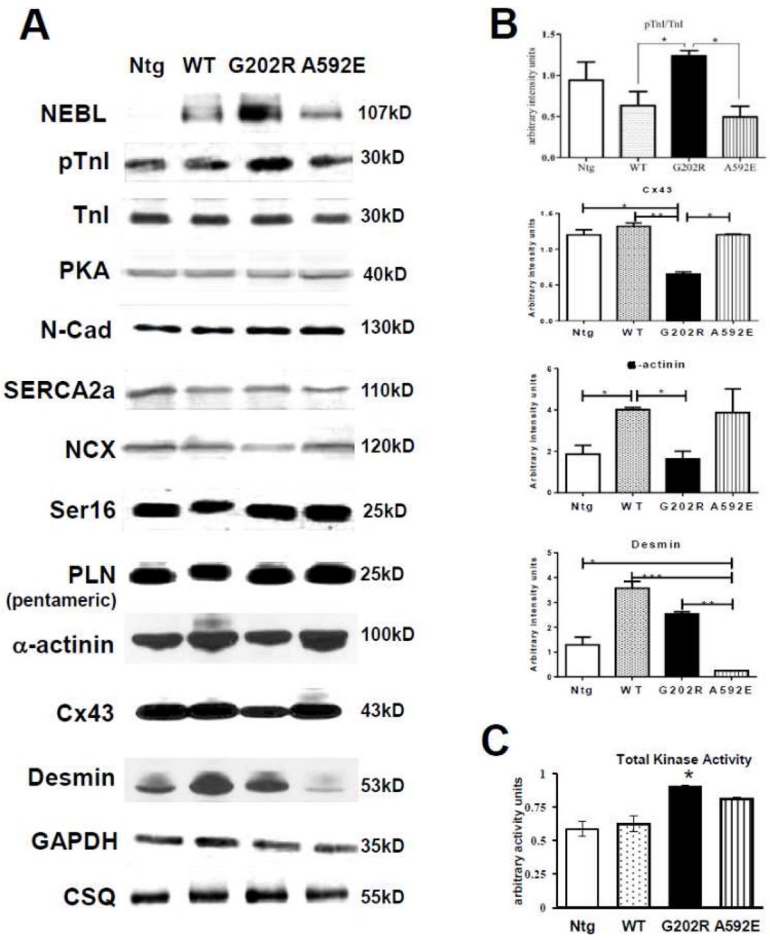

Figure 4. Protein expression in heart lysates of 3 month old non-Tg and NEBL-Tg mice

A) Results of Western blotting performed in whole heart lysates from 3-month-old mice. Expression of NEBL transgene was determined prior to experiments. B) Quantification indicated increased $Ser^{23/24}$ cTnI phosphorylation (pTnI) and decreased Cx43 in G202R-Tg lysates. α-actinin was decreased in G202R-Tg compared to WT-Tg. Desmin expression was significantly decreased in A592E-Tg compared to all groups. Densitometry performed with Image J, n=4–5/group. C) Total kinase activity increased in the G202R-Tg group compared to control non-Tg and WT-Tg groups, n = 4/group.

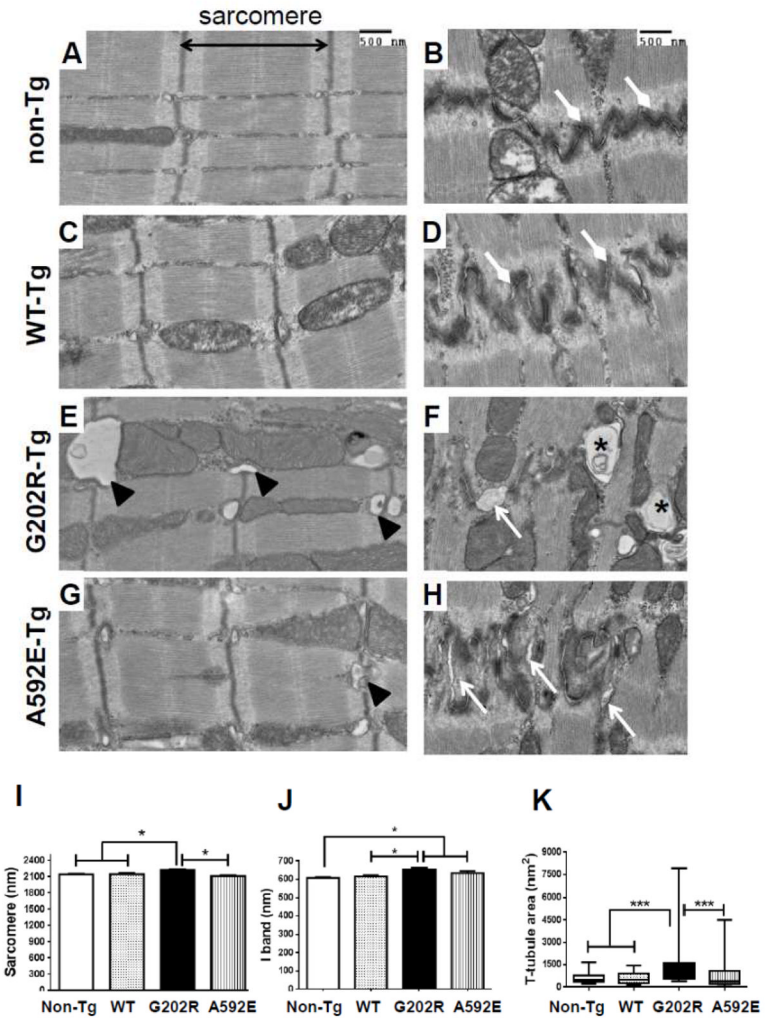

Figure 5. Myocardial ultrastructure at 3-month-old mice

A–H) Left column represent images of LV myocardial sarcomeres and I-band, right columns represent intercalated discs at cell-cell junction in non-Tg (A-B), WT-Tg (C–D) and G202R-Tg (E–F) and A592E-Tg (G–H) mice. Non-Tg and WT-Tg myocardium shows comparable sarcomere and I-band length and tightly connected cell-cell junctions (diamond head arrows). The G202R-Tg myocardium shows desmosome separation (block arrow) and cell-cell membrane disruption (asterisks). The A592E-Tg myocardium shows intercalated disruption (arrows), but to a lesser degree than G202R-Tg. I) Analysis of sarcomere length indicates increased in G202R-Tg mutants compared to non-Tg, WT-Tg, and A592E-Tg. J) I-band length was increased in both mutants compared to non-Tg. K) T-tubule area was increased in G202R-Tg cardiomyocytes compared to all groups. N=2–4 hearts in each group, at least 100 sarcomeres from 10 sections per heart examined. Measurements made using Image J. Scale bar = 500 nm. *=P<0.05 compared to control of the same genotype. Data analyzed by Mann-Whitney t-test.

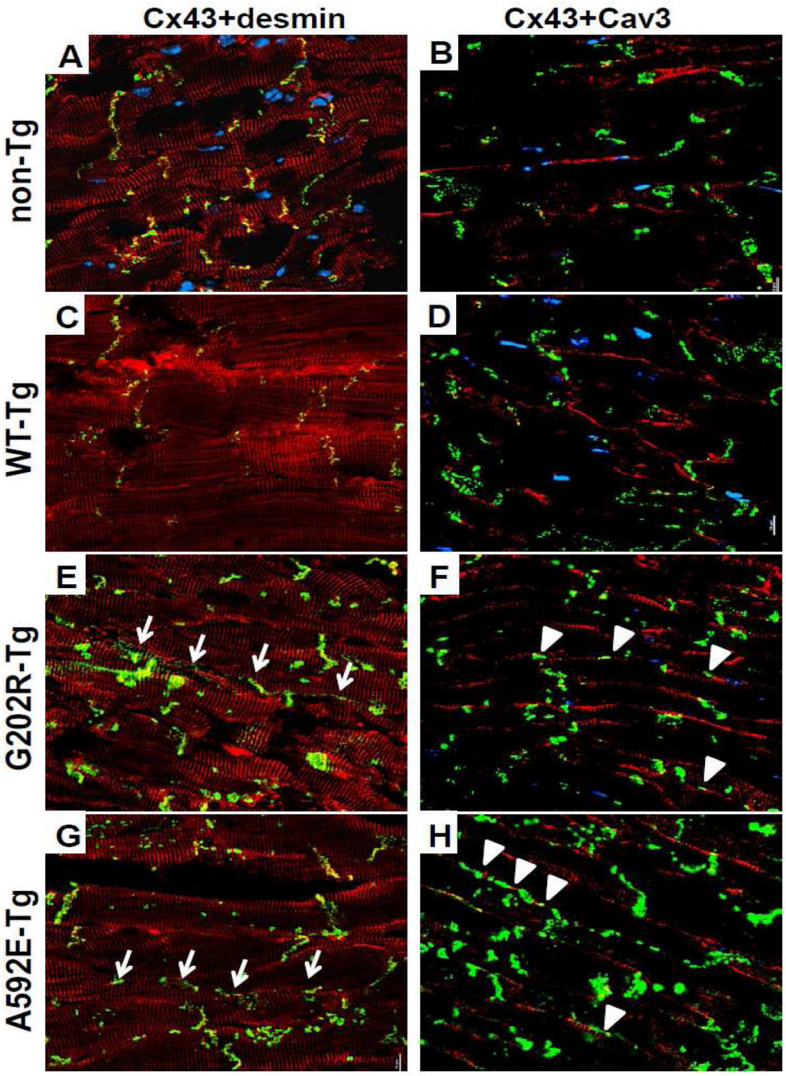

Figure 6. Immunohistochemical analysis of ventricular myocardial sections from 3-month old non-Tg and NEBL-Tg mice

5μm thick longitudinal cryosections of left ventricle tissue were examined for the expression of desmin, Cx43, and Cav3. Left columns: Cx43 (green) co-localized with desmin (red) at the intercalated disc in non-Tg (A) and WT-Tg (C) cardiomyocytes (co-localization is indicated by yellow color), but Cx43 was mislocalized to the lateral myocardial border (arrows) in G202R-Tg (E) and A592E-Tg (G) tissues. Desmin was expressed at the Z-disc and intercalated disc similarly in all groups. Right columns: Cav3 (red) and Cx43 (green) were co-stained. Cav3 is localized to the lateral borders of sarcolemma, while Cx43 is visualized in intercalated discs of non-Tg (B) and WT-Tg (D) cardiomyocytes. Cx43 expression showed lateralization and colocalization (arrowheads) with Cav3 in both NEBL mutants (F and H). Cx43= connexin 43; Cav3= caveolin 3. n=3, number of slides per heart analyzed, N=2, number of hearts analyzed per group.

Table 1

Major phenotypic differences found in NEBL transgenic mutant mice compared to non-Tg and WT-Tg controls at 3 months of age

Geometric constant was increased in both mutants compared to control non-Tg littermates and WT-Tg mice. Mechanical behavior showed decreased torsion in G202R-Tg hearts and increased twist and untwisting rate in A592E-Tg hearts. Increased calcium decay rate and pTnI expression were detected in G202R-Tg cardiomyocytes and heart lysates, respectively. Cx43 was downregulated in G202R-Tg, whereas desmin expression decreased in A592E-Tg hearts. Sarcomere and I-band length was significantly increased in G202R-Tg. Structural abnormalities seen in both mutants were intercalated disc separation, t-tubule disorganization and enlargement, and Cx43 lateralization. T-tubule enlargement was significant in G202R-Tg myocardium compared to other groups.

Mouse Type	*In vivo* mechanical behavior			*Ex vivo* mechanical behavior	*Ex vivo* calcium behavior	Protein Expression			Structural Alterations		
	Torsion (°)	Twist (°)	Geometric Constant	Untwisting rate (°/sec)	Calcium decay (1/τ)	pTnI	Cx43	Desmin	I-band/sarcomere length	Desmosome separation	T-tubule enlargement
Non-Tg	n.d.	n.d.	n.d.	n.d.	n.d	n.d.	n.d.	n.d.	n.d.	no	no
WT-Tg	n.d	n.d	n.d.	n.d.	n.d.	n.d.	n.d.	↑*§	n.d.	no	no
G202R-Tg	↓*§	n.d.	↑*§	n.d.	↑§	↑*§	↓*§	↑*	↑*§	Yes + Cx43 lateralization	yes *§
A592 E-Tg	n.d.	↑*§	↑*§	↑§	n.d	n.d.	n.d.	↓*§	n.d.	Yes + Cx43 lateralization	yes

↑ =increase; ↓ =decrease; n.d.=no difference from Non-Tg or WT-Tg;

* indicates a significant ($p<0.05$) change from non-Tg;

§ indicates a significant ($p<0.05$) change from WT-Tg.

J Mol Cell Cardiol. Author manuscript; available in PMC 2014 July 01.